



Localization of the Gamma-Ray Emission Region in the 1 September 2014 Behind-the-Limb Solar Flare According to the *Fermi*/LAT Data

A.A. Kochanov¹ · V.I. Kiselev¹ · V.V. Grechnev¹ · A.M. Uralov¹

Received: 7 July 2023 / Accepted: 26 January 2024
© The Author(s), under exclusive licence to Springer Nature B.V. 2024

Abstract

Since the launch of the *Fermi* mission in 2008, it has become possible to study high-energy solar γ -rays with an unprecedented imaging capability. In particular, the position of the > 100 MeV γ -ray source can shed light on the origin of high-energy protons that is still controversial. However, the imaging of solar γ -ray sources with the *Fermi Large Area Telescope* (LAT) is a complex multi-stage process influenced by a number of factors and instrumental effects, which is difficult to fully comprehend a priori. The SOL2014-09-01 behind-the-limb event was significant, for which the γ -ray source position was not firmly established at once. Following the methodology outlined by the *Fermi*/LAT team, we estimated the proton power-law indices and γ -ray centroid positions at two temporal intervals of this event, separated by one hour. Our estimates for the first interval are comparable to estimates recently updated by the *Fermi*/LAT team, thereby confirming the consistency of the analysis applied. Although, in the second interval, corresponding to the decay phase of the flare, the proton power-law index clearly hardened, the presumable position of the fading γ -ray source remained unchanged. Its constancy in both temporal intervals and its proximity to the bases of long coronal loops connected to the flare site support the flare origin of high-energy protons injected into these loops along with electrons and trapped there for a long time. Our experience analyzing *Fermi*/LAT data clarifies their complex handling and will hopefully benefit the solar community in their wider use.

Keywords Energetic particles, protons · Flares, energetic particles · Gamma-ray emission

✉ A.A. Kochanov
kochanov@iszf.irk.ru

V.I. Kiselev
valentin_kiselev@iszf.irk.ru

V.V. Grechnev
grechnev@iszf.irk.ru

A.M. Uralov
uralov@iszf.irk.ru

¹ Institute of Solar-Terrestrial Physics SB RAS, Lermontov St. 126A, Irkutsk 664033, Russia

1. Introduction

Solar storms generate many phenomena, some strong enough to produce considerable space-weather disturbances. These disturbances can disrupt the operation of various ground-based and space-borne systems and threaten to human activities and health. One of the types of space-weather disturbances is solar energetic particles (SEPs). Their significant part is protons accelerated to energies, usually from fractions of a MeV to tens or hundreds of MeV and reaching up to several GeV in ground-level events (GLEs). Elucidation of the sources of accelerated protons is important both for practical forecasting and warning of their appearance and for understanding the processes of charged-particle acceleration in solar and space plasmas.

Two types of possible particle accelerators have long been known: flare processes in solar active regions and shock waves associated with coronal mass ejections (CMEs). The manifestations of electrons accelerated in flares are diverse and beyond doubt. In contrast, remote observations of accelerated protons are possible only by the γ -ray emission that appears in nuclear reactions with their participation and can be identified by the shape of its spectrum. This circumstance complicates the identification of the proton-acceleration process and its localization.

The γ -ray nuclear de-excitation lines were first observed by Hirasima, Okudaira, and Yamagami (1970) in the SOL1968-09-27 flare. Since then, the temporal profiles and spectra of nuclear γ -ray emission have been measured in detail (e.g., Vilmer, MacKinnon, and Hurford, 2011). During the era of observations with the *Reuven Ramaty High-Energy Solar Spectroscopic Imager* (RHESSI: Lin et al., 2002), images were obtained in the 2.223 MeV neutron-capture line for a number of flares. They revealed the positions of the γ -ray sources in the flaring active regions not far from the hard X-ray electron-bremsstrahlung sources. This location, along with other observational facts, indicates the acceleration of protons to several tens of MeV in flaring active regions by processes closely related to the acceleration of electrons (Vilmer, MacKinnon, and Hurford, 2011).

The greatest uncertainties relate to the origin of high-energy protons. They can be manifested due to collisions with ambient solar nuclei that generate secondary neutral and charged pions if the energy of incident protons exceeds 300 MeV. The pions rapidly decay, producing the γ -ray emission whose spectrum is a broad plateau in the 30–150 MeV energy range (e.g., Murphy, Dermer, and Ramaty, 1987; Chupp and Ryan, 2009).

The π -decay emission at photon energies > 100 MeV was first detected in the SOL1982-06-03 event (Chupp et al., 1982). Two phases of the π -decay emission have been distinguished. The first, impulsive phase is clearly associated with a flare. The second phase is a long-duration emission that can persist for hours after the flare. One or both of these phases were observed later in several flares (e.g., Share et al., 2018; Ajello et al., 2021a). To explain the long-duration γ -ray emission, prolonged acceleration and trapping have been proposed (e.g., Mandzhavidze and Ramaty, 1992; Akimov et al., 1996; Ryan, 2000).

The challenge for the flare origin of accelerated protons is the γ -ray emission observed in some events when the flare site is behind the limb. To explain the γ -ray-line emission in the occulted SOL1989-09-29 flare, Cliver, Kahler, and Vestrand (1993) proposed that protons accelerated by a CME shock on an open magnetic field partly escaped into the interplanetary space and partly returned to the solar surface, precipitating far from the flare region. This idea has also been invoked to interpret recent behind-the-limb flares followed by a sustained π -decay emission (Pesce-Rollins et al., 2015a,b; Ackermann et al., 2017).

Essential information for identifying a probable source of high-energy protons can be the location of the source of the γ -ray emission they produce. One could only guess about

the localization of sources of high-energy γ -rays until the launch of the *Fermi* mission in 2008. Now, with the main purpose of studying galactic and extragalactic γ -rays, the *Fermi Large Area Telescope* (LAT: Atwood et al., 2009) has also made it possible for the first time imaging observations of solar γ -rays with energies greater than 60 MeV.

The nominal LAT 68%-containment radius for a single on-axis γ -ray photon is 3.0° for 100 MeV and 0.4° for 1 GeV (these quantities refer to the best quality of the reconstructed direction). The γ -ray source is localized by calculating its emission centroid position. The more registered photons are, the more accurately their source is localized. *Fermi*/LAT imaging of solar γ -ray sources is a sophisticated process that includes several sequential steps influenced by a number of factors, as well as instrumental effects and algorithms. Some could be understood only during data handling and comprehending its results, which were subsequently refined.

Of the three behind-the-limb flares observed by *Fermi*/LAT, the most powerful was the SOL2014-09-01 event so that the accuracy of the localization of the γ -ray source in this event was expected to be the highest. This event was remarkable in several respects. In particular, it gave rise to the fastest CME (1900 km s^{-1} according to the online CME catalog cdaw.gsfc.nasa.gov/CME_list/; Yashiro et al., 2004) among these three events and produced a strong SEP event whose parameters were comparable to or even surpassed the typical SEPs that caused GLEs (Plotnikov, Rouillard, and Share, 2017; Cohen and Mewaldt, 2018; Gopalswamy et al., 2020). For these reasons, this event has attracted the attention of researchers (e.g., Hudson, 2018; Jin et al., 2018 in addition to the articles just mentioned).

Ackermann et al. (2017) found in this event the centroid position of the > 100 MeV γ -ray emission on the northeastern limb far from both the flare site and the region of gyrosynchrotron emission, whose connection with the flare site was highly probable. Grechnev et al. (2018) established that the area of this centroid position was covered by a dense system of short closed loops that had no connection with the flare site. Hence, neither flare-accelerated nor shock-accelerated protons could have access to this region. Considering the result of Ackermann et al. (2017) to reflect the real spatial distribution of γ -ray photons, Grechnev et al. (2018) assumed that the centroid position was displaced from the major generation region of the pion-decay emission due to the contribution of secondaries produced in a dense coronal streamer. This contribution was presumably noticeable mainly at lower energies, and, therefore, it was expected that the γ -ray emission centroid position would depend on the lower threshold of photon energy [E_γ^{cut}] that were taken into account in its calculation.

Indeed, our first calculations from LAT data revealed a clear dependence of the centroid position on the lower-energy threshold (Grechnev et al., 2018). With an increase in E_γ^{cut} from 100 to 300 MeV, the centroid position shifted strongly towards the bases of the coronal loops connected to the flare site. Ajello et al. (2021a) succeeded in elucidating that this displacement was caused by a selection bias in the LAT trigger and reconstruction algorithms (the “fish-eye effect”). The effect depends on the energy and incident angle of the γ -ray photon. Using the automated localization tool SunMonitor, Ajello et al. (2021a) determined the refined > 100 MeV emission centroid position of $X = -1005''$, $Y = -182''$ in the temporal window 11:02–11:18. Note that the > 100 MeV emission centroid positions for almost all of the events listed in the LAT catalog are remarkably close to their parent active regions (except for the 7 March 2012 event). It is also of interest whether the > 100 MeV emission centroid position remained stable in the 1 September 2014 event or whether it evolved during the late phase.

We attempted to find the position of the γ -ray-emitting region in the 1 September 2014 event, following the methodology outlined by Ajello et al. (2014) and Ackermann et al. (2017). In the process, we found that some required steps and parameters were not obvious,

and the procedure for calculating the γ -ray emission centroid position was very complex. We obtained results comparable to those updated by the *Fermi*/LAT team for the temporal window they considered, thereby confirming the consistency of our analysis. According to Share et al. (2018), in this event, the late-phase >100 MeV γ -ray emission lasted up to 6 hours. We also succeeded in determining the γ -ray emission centroid position for one of the late-phase intervals suitable for the analysis. Our experience in handling *Fermi*/LAT data appears to be helpful to the solar community. This is especially important because *Fermi* is currently the only mission able to detect high-energy emission from the Sun (Longo, Iafra, and Fermi LAT Collaboration, 2011).

We address the stages of the localization procedure for the γ -ray-emitting region in the 1 September 2014 event as follows. Section 2 describes the retrieval, selection, and preprocessing of raw LAT data, construction of the spectral and spatial models, and calculations of the γ -ray spectra in two temporal intervals on the basis of the likelihood analysis. Section 3 addresses the γ -ray emission centroid position for the two temporal intervals and discusses its possible relation to the existing coronal configuration. Section 4 summarizes the results.

2. Spectral Analysis

2.1. Selection Criteria for *Fermi*/LAT Data

The *Fermi*/LAT data were retrieved via the Web query form fermi.gsfc.nasa.gov/cgi-bin/ssc/LAT/LATDataQuery.cgi. We processed the LAT spectra using the Fermi Science Tools software package as well as user contributions accessible at fermi.gsfc.nasa.gov/ssc/. The processing was based on the latest version of Pass 8 R3 data, following the methodology described by Ajello et al. (2014) and Ackermann et al. (2017).

From the analysis of spacecraft orbits (the `glg_poshist_all_140901_v01.fit` file with the orbital history for the 1 September 2014 event), two temporal intervals 11:02–11:18 and 12:25–12:57 were determined (all times hereafter are referred to UTC), when the LAT boresight was directed towards the Sun and the number of detected γ -ray photons with energy $E_\gamma > 60$ MeV exceeded the background level by at least several times. The intervals were chosen from the condition that the Sun was within an angle of $\leq 70^\circ$ from the LAT boresight. The first observation interval, in which the main flux of the flare γ -ray emission was recorded, was as short as 16 min. The Sun was observed near the boundary of the limiting angles for the analysis of $65 - 70^\circ$, where the detector response is low and less accurately determined. This led to the exceptional complexity of reconstructing the γ -ray emission centroid position in this event by Ackermann et al. (2017) and Ajello et al. (2021a,b). The second interval falls on the decay phase of the γ -ray emission, when the Sun was observed on average at angles of about 50° with respect to the LAT boresight.

We selected for the analysis events within a radius of 10° from the Sun's center that satisfied the attribute of the Source class and the Front/Back detector conversion type. These γ -ray-like events were subjected to reconstruction and classification algorithms in the LAT detector and, with some probability (including misclassified events), were identified by the *Fermi*/LAT software as γ -ray photons. To suppress the diffuse contribution of the γ -ray emission of the Earth's atmosphere, the condition `zmax = 90` was applied, where `zmax` is the maximal angle between the reconstructed direction of the event and the zenith line passing from the Earth's center through spacecraft. To exclude intervals where the data were marked as Bad, the events were subjected to an additional logical filter (`DATA_QUAL>0`)&&(LAT_CONFIG==1). As a result, the number of events that passed the specified criteria was 3353 for the first interval, and 201 for the second.

2.2. Construction of the Spectral and Spatial Models

At energies of γ -ray photons of > 60 MeV in the 1 September 2014 event, a broad π -decay emission line dominates over the electron bremsstrahlung continuum. Basically, these are γ -ray emission from the prompt decay of neutral pions ($\pi^0 \rightarrow 2\gamma$) and a fraction of γ -ray emission of positrons and electrons generated in the decay chains of charged pions and muons ($\pi^\pm \rightarrow \mu^\pm + \nu_\mu$, $\mu^+ \rightarrow e^+ + \nu_e + \bar{\nu}_\mu$, $\mu^- \rightarrow e^- + \bar{\nu}_e + \nu_\mu$) (Dermer, 1986; Murphy, Dermer, and Ramaty, 1987). In the analysis of the spectrum, we use the results of numerical calculations by Murphy, Dermer, and Ramaty (1987) taken from the OSPEX distributive set (Tolbert and Schwartz, 2020) as a fitting function for the π -decay emission. The calculations include a series of the so-called π -decay templates of γ -ray emission obtained from a detailed analysis of the interactions of accelerated protons with a thick target in a magnetic field of 300 G. The spectrum of incident accelerated protons was assumed to have a power-law shape $\propto E^{-\beta}$ with an isotropic pitch-angle distribution. The calculation was performed on a grid of proton power-law indices β from 3 to 5 in steps of 0.01.

The isotropic contribution of extragalactic diffuse γ -rays, spatially unresolved extragalactic sources, and cosmic rays not classified at the output of processing was taken into account by the spectral model iso_P8R3_SOURCE from the catalog of background models accessible at fermi.gsfc.nasa.gov/ssc/data/access/lat/BackgroundModels.html. The contribution of the diffuse galactic γ -ray emission, due to the low exposure, was taken into account by the same isotropic background model in which the normalization was assumed to be a free parameter. The nonthermal quiet-Sun's γ -ray emission was considered in terms of the empirical model by Abdo et al. (2011).

The complete model includes information about the spatial position of the flare source and the background of the solar disk. The position of the solar disk in the Geocentric Celestial Reference System (GCRS) was calculated for the middle of the selected temporal window. The position of the γ -ray flare source was unknown at this stage of the analysis and is set at the solar-disk center. Both sources were considered to be point sources. Ajello et al. (2021a) estimated the actual dimensions of the γ -ray flare sources in the two brightest flares on 7 March 2012 and 10 September 2017 using two spatial templates, a flat disk and a Gaussian source. In both cases, no statistically significant signs indicating spatial broadening were found. The authors put an upper limit on the size, which turned out to be less than the solar-disk radius. These two events are the only sufficiently bright flares detected by LAT for which it was possible to perform such an analysis.

2.3. Likelihood Analysis: Folded and Unfolded Spectra

The fitting of the parameters of the signal and background models to the observations was carried out in the framework of an unbinned analysis with the maximum likelihood optimization technique (see, e.g., Mattox et al., 1996; Abdo et al., 2009). The fitting process was performed on the grid of values of the desired proton spectrum index β . As a result, that realization of the calculated π -decay spectrum was chosen that gave the maximum agreement with the observed spectrum. Next, the centroid position of the flare source was found using the method described in Section 3, the coordinates in the source model were refined, and the optimal parameters of the proton spectrum were calculated again.

Figures 1a and 1b show the spectra of the raw count rate of the LAT detector for two selected temporal windows compared with the results of fitting the signal and background models. As Figure 1a shows, the γ -ray emission produced by the event had practically no background in the first observation interval. In the second interval, the total contribution of

Figure 1 The spectra of the LAT count rate (*filled circles*) during two temporal intervals of 11:02–11:18 (a) and 12:25–12:57 (b) compared with model calculations. The *pink curve* is the count rate according to the galactic and extragalactic isotropic background model, the *green curve* is the prediction of the quiet-Sun model, and the *blue curve* represents the spectrum of the π -decay emission. The *red curve* represents the complete model.

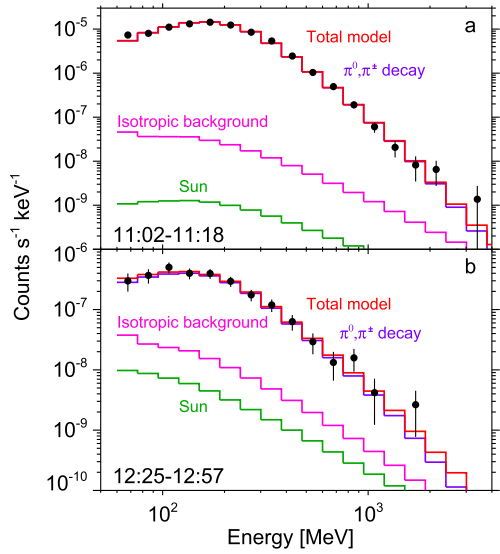
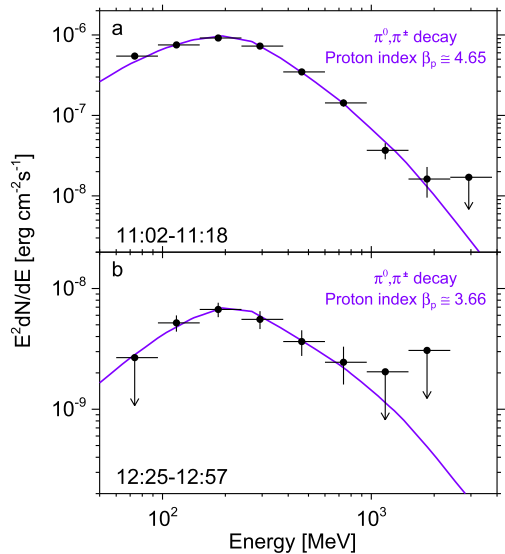


Figure 2 Reconstructed energy spectra of the background-subtracted γ -ray emission (*filled circles*) for the two temporal intervals of 11:02–11:18 (a) and 12:25–12:57 (b). The *blue curves* represent the prediction of the π -decay-emission model.



the isotropic background and quiet-Sun models was $< 1\%$ at $E_\gamma = 100$ MeV and reached 35% at the upper edge of the considered energy range.

Figure 2 shows reconstructed energy spectra of the background-subtracted γ -ray emission. The spectra were obtained using the user-contributed procedure likeSED from the Fermi software repository. The data were divided into 10 equal (on a logarithmic scale) energy intervals in the energy range from 60 MeV to 6 GeV. In each interval, the emission flux was restored. The spectrum of a point source within the interval followed the power law E_γ^{-2} . The background-model parameters were fixed at their optimal values found from the analysis of the folded spectra. The reconstructed energy spectra (data points) and pa-

Table 1 Results of spectral analysis of the π -decay emission in the 1 September 2014 event.

Temporal interval	Exposure time [minutes]	Flux > 100 MeV [10^{-5} phot. cm^{-2} s^{-1}]	Proton index
11:02 – 11:18	16	403 ± 7	4.65 ± 0.08
12:25 – 12:57	32	2.9 ± 0.2	3.7 ± 0.2

parameters of the π -decay-emission model were found in some sense independently from the folded spectra; however, the agreement between the data and the model within the measurement errors indicates the consistency of the performed analysis.

Table 1 presents the numerical results of the spectral analysis. The total fluxes of the > 100 MeV γ -ray emission and the reconstructed power-law spectral indices of accelerated protons generally agree with the estimates of previous years. Based on the joint spectral analysis of the *Fermi Gamma-ray Burst Monitor* (GBM; Meegan et al., 2009) and LAT data, Ackermann et al. (2017) estimated the proton spectrum index for the first interval of Table 1 to be 4.4. The total flux estimated from the LAT data in the interval of 11:04 – 11:18 was 435×10^{-5} photons cm^{-2} s^{-1} . Share et al. (2018) considered three intervals of 11:06 – 11:12, 11:12 – 11:20, and 12:26 – 12:58 and estimated total fluxes of 400, 500, and 3.0 (in the same units) with corresponding proton indices of 4.75, 4.35, and 3.65, respectively. Kafexhiu et al. (2018) processed the LAT data based on revised calculations of hadronic γ -ray emission for both protons and heavier nuclei. These authors obtained the hardest proton spectrum of 3.71 for the interval 11:02 – 11:18. Ajello et al. (2021a) presented refined results of the spectral analysis that the *Fermi/LAT* collaboration made for this flare. For two intervals of 11:02 – 11:18 and 12:25 – 12:57, the total fluxes of the > 100 MeV γ -ray emission were estimated to be 379 and 2.98 with the corresponding proton indices of 4.7 and 3.72.

3. The γ -Ray Emission Centroid Position Calculated from the LAT Data

3.1. Calculations and Results

In the following steps, we aim to reproduce the updated results of Ajello et al. (2021a) and estimate the centroid position for the 12:25 – 12:57 interval, while being mindful of potential localization issues. To find the γ -ray emission centroid position, we use the `gttmap` and `gtfindsrc` procedures from the *Fermi Science Tools* package. At the first stage of localization, `gttmap` is used to calculate the test-statistics map $\text{TS}_{(\text{RA}, \text{Dec})} = -2 \ln[\mathcal{L}_0^{\text{max}} / \mathcal{L}_1^{\text{max}}]$ on a rectangular coordinate grid “right ascension (RA), declination (Dec)”. Here, $\mathcal{L}_0^{\text{max}}$ is the maximum likelihood value for the model without a source (null hypothesis) at each grid node, and $\mathcal{L}_1^{\text{max}}$ is the value for the model with an additional source (alternative hypothesis). The null hypothesis is a background model with fixed parameters found at the first iteration of the spectral analysis. Here, a point source with a power-law spectrum plays the role of the alternative hypothesis. The maximum on the TS map corresponds to the desired location of the test source since higher TS values indicate a greater significance of the alternative hypothesis. In our case, the TS map values for both temporal intervals well exceeded the 5σ source-detection level.

From the preliminary analysis of the TS map calculated for the first temporal interval without the fish-eye correction, we observed a strong shift in the γ -ray emission centroid position when the energy threshold E_γ^{cut} was lowered (we selected 300, 100, and 60 MeV).

The shift exceeded 68% confidence radius towards the LAT boresight. The source location with $E_{\gamma}^{\text{cut}} = 300$ MeV had the smallest dispersion of coordinates.

In the second temporal interval, the influence of the fish-eye effect is minor. In the PASS 8 data release, the *Fermi* collaboration has introduced the `fisheye_correction` extension in the Instrument Response Functions that contains tables for quantifying the offset angle in LAT polar coordinates. Currently, the *Fermi* standard data-processing tools do not support the effect correction. Following the description of Ackermann et al. (2012) in their Section 6.4, we use these tables to assess the systematic-bias effect by ourselves.

The *Fermi*/LAT team provides three different methods for quantifying the fish-eye bias. These are the MEAN, MEDIAN, and PEAK of a Gaussian fit to a modeled offset-angle distribution. At large boresight angles of $\gtrsim 70^\circ$, these values may differ noticeably from each other, especially in the low-energy region. Therefore, the final difference between the corrected and uncorrected positions at different low-cutoff energies depends on this choice. We developed an algorithm that not only computes the magnitude of the fish-eye correction for utmost cases (like MEAN or PEAK) but also can linearly scale between them, giving the user more freedom. Using this algorithm, we obtained the magnitude of the fish-eye correction that minimized the distance between the corrected centroid positions found with different energy thresholds for the first temporal interval of the event. For the second temporal interval with a favorable boresight angle of about 50° , it was sufficient to use only the MEAN table. We use it as the default option unless complications such as those discussed arise.

Our entire scheme for calculating the centroid position is as follows. The true position of the γ -ray source is initially unknown, and it is forced to be placed at the well-known solar-disk center (Section 2.2). Then, we apply a fish-eye correction to each event retrieved from a *Fermi*/LAT photon file. Correction for the motion of the Sun within small temporal intervals < 30 min is not mandatory, although it is performed in our analysis. After obtaining the approximate γ -ray emission centroid position, which was offset from the solar-disk center, we refine our source model with new coordinates and repeat the calculation loop from the very beginning. In our experience, two or three passes are sufficient to ensure the stability of the result. We run three independent calculations in the same way for different input E_{γ}^{cut} thresholds of 60, 100, and 300 MeV, following the notion of the *Fermi*/LAT team that the distance between corrected and uncorrected positions is expected to decrease with increasing energy (see, e.g., Figure 4 in Ajello et al., 2021a).

Figures 3a and 3b present the γ -ray emission centroid positions calculated using `gttsmap` procedure and fish-eye corrected γ -ray data. The coordinates for the three E_{γ}^{cut} values are comparable and within the estimated 68% confidence intervals. The `gtfindsrc` tool was used to find the best estimate of the position of the presumable source. Figures 3c and 3d show the final centroid position found using the `gtfindsrc` tool and the π -decay-emission model.

The amount of displacement due to the fish-eye effect is shown by the initial > 100 MeV emission centroid position found by Ackermann et al. (2017) (gray dot and circle), who did not apply the correction. The `gtfindsrc` procedure gives an error radius of 68%, so the confidence intervals are represented by circles, unlike ellipses in TS maps. As the figure shows, taking into account the π -decay-emission spectral model leads to an even smaller dispersion of the coordinates with different cutoff energies. The presumable position of the γ -ray source seems to be constant in the two temporal intervals separated by one hour, while the proton power-law index hardened from 4.7 to 3.7. The γ -ray source position in the second interval is less affected by the fish-eye effect, though the estimated 68% error radius is considerably larger because of the low photon statistics.

Our localization results are summarized in Table 2. The elliptic confidence intervals of 68% and 90% estimated from the TS maps are listed in the table as the geometric mean of their semi-axes.

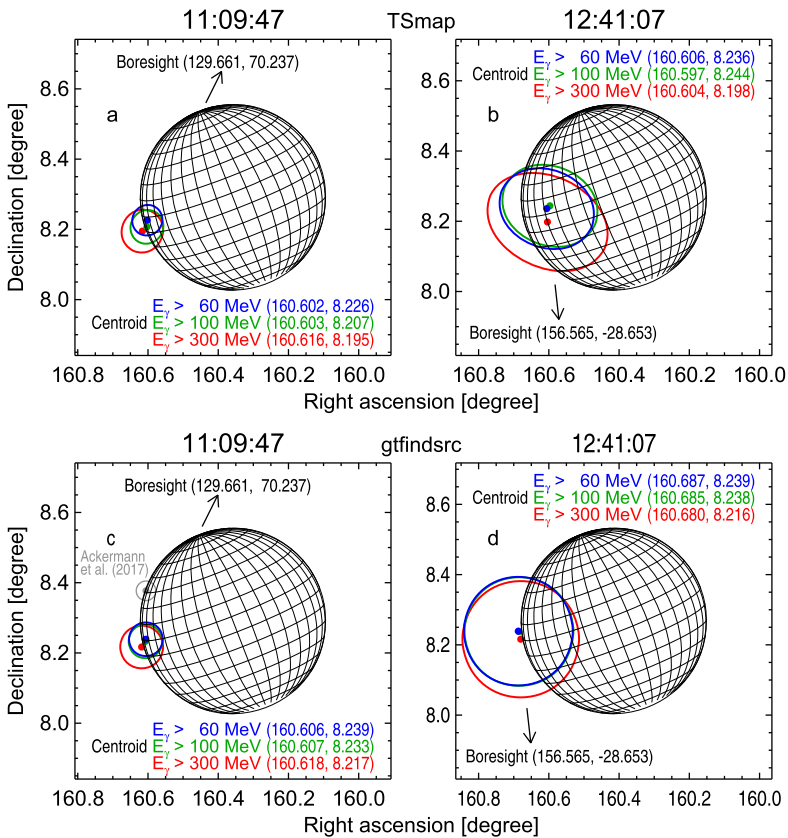


Figure 3 The γ -ray emission centroid positions calculated for two temporal intervals 11:02–11:18 and 12:25–12:57. The 68 % location uncertainty regions are indicated by ellipses for three low-energy cuts of 60, 100, and 300 MeV. Panels **a** and **b** show the centroid locations calculated using the TS map and a power-law point-source model; panels **c** and **d** show the optimized centroid positions using the pion-decay model and the gtfndsrc procedure. The gray dot and circle present the initial > 100 MeV emission centroid position from Ackermann et al. (2017), not corrected for the fish-eye effect. The arrows indicate approximate directions to the LAT boresight. The positions of the Sun's center are calculated for the mean time of each interval.

3.2. Comparison of the Results with Existing Coronal Configuration

Let us now compare the results of calculations with observations. Figure 4 (similar to a combination of Figures 5 and 6 in Grechnev et al., 2018) presents colored uncertainty circles of the calculated γ -ray emission centroid positions along with flare-related manifestations visible in radio emission, coronal structures actually observed in the extreme ultraviolet (EUV), and the coronal magnetic field extrapolated in the potential approximation.

The halftone background in Figure 4a is a pre-event combined EUV image. Its higher-contrast central part was composed of a set of 171 \AA images obtained during 10:56–10:58 with the *Atmospheric Imaging Assembly* (AIA: Lemen et al., 2012) on board the *Solar Dynamics Observatory* (SDO: Pesnell, Thompson, and Chamberlin, 2012). The lower-contrast periphery, extending the SDO/AIA field of view, was composed of 174 \AA images obtained in a close temporal interval with the *Sun Watcher using Active Pixel system detector and image processing imager* (SWAP: Berghmans et al., 2006) on board the *Proba 2* micro-satellite.

Table 2 SOL2014-09-01 γ -ray centroid position coordinates.

E_{γ}^{cut} [MeV]	RA, Dec ^a		X, Y^b		$r68\%$		$r90\%$
	[degree]		[arcsec]		[arcsec]		
	TS ^c	GF ^d	TS	GF	TS	GF	TS
11:01:57 – 11:17:38 (mean 11:09:47) ^e							
60	160.602, 8.226	160.606, 8.239	−905, 97	−900, 147	155	173	230
100	160.603, 8.207	160.607, 8.233	−932, 37	−911, 129	173	173	241
300	160.616, 8.195	160.618, 8.217	−989, 12	−969, 89	216	220	292
12:24:55 – 12:57:19 (mean 12:41:07) ^f							
60	160.606, 8.236	160.687, 8.239	−684, 142	−951, 256	443	558	626
100	160.597, 8.244	160.685, 8.238	−641, 157	−946, 250	454	558	634
300	160.604, 8.198	160.680, 8.216	−725, 8	−957, 170	547	598	770

^aGeocentric Celestial Reference System

^bHelioprojective cartesian coordinates

^cTS = gttsmmap procedure generates a test-statistics map

^dGF = gtfndsrc procedure optimizes a point-source location using the likelihood test-statistics

^eSolar-disk center (160.358, 8.291), LAT boresight (129.661, 70.237)

^fSolar-disk center (160.415, 8.268), LAT boresight (156.565, −28.653)

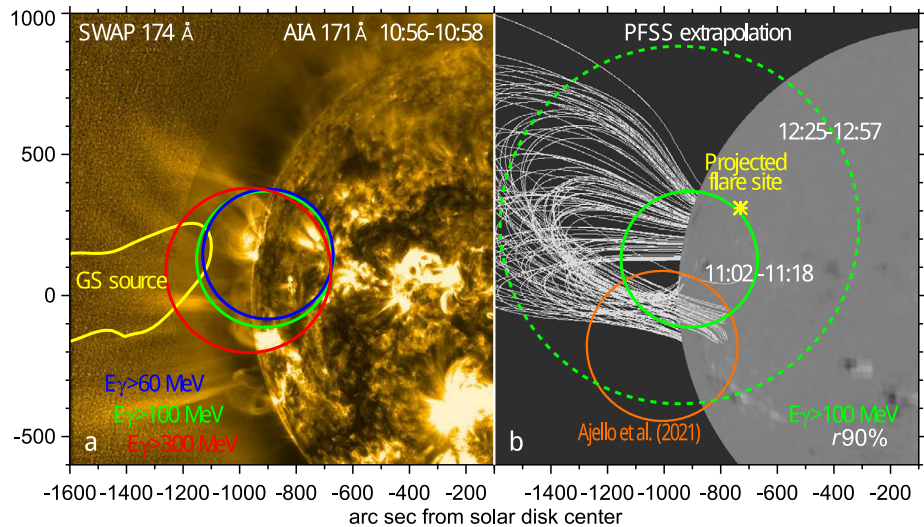


Figure 4 The γ -ray emission centroid positions with respect to the radio and EUV data and magnetic-field extrapolation. Left (a): the 90 % centroid location uncertainty regions (circles) calculated for the interval 11:02 – 11:18 and three low-energy cuts of γ -ray photons of 60, 100, and 300 MeV. The yellow contour presents the gyrosynchrotron (GS) source according to the NRH data at 432 MHz. The background half-tone image shows a system of high coronal loops observed in EUV. The image was composed of the SDO/AIA 171 Å and Proba 2/SWAP 174 Å data set obtained in the close temporal interval of 10:56 – 10:58. Right (b): the loop structure of the coronal magnetic field reconstructed using the PFSS model. The field lines connect the flaring region behind the limb (yellow star) with the visible solar surface. Green circles are the results of calculating the > 100 MeV emission centroid positions for two temporal intervals 11:02 – 11:18 (solid) and 12:25 – 12:57 (dotted). The brown circle represents the > 100 MeV emission centroid position established by Ajello et al. (2021a) with uncertainty error radius scaled to 90%.

The yellow contour in Figure 4a presents the main gyrosynchrotron (GS) source observed by the Nançay Radioheliograph (NRH: Kerdraon and Delouis, 1997) at 432 MHz (40% level or 0.2 MK). This static long-lived GS source was associated with the far-side flare. Its lower portion near the limb was probably suppressed because of refraction. The temporal profile of the GS emission indicated long-term trapping of emitting accelerated electrons that were most likely injected from the flare site into long loops (see Grechnev et al., 2018 for details).

Figure 4b presents the loop structure of the coronal magnetic field that was extrapolated using the *Potential Field Source Surface* model (PFSS: Schrijver and De Rosa, 2003) from a synoptic magnetogram. This magnetogram was produced from a set of magnetograms observed with the *Helioseismic and Magnetic Imager* (HMI: Scherrer et al., 2012) on board SDO. The photospheric bases of the field lines were chosen in such a way as to ensure the magnetic connection of the flaring region behind the limb (yellow star) with the visible solar surface. Note that synoptic magnetograms may somewhat differ from the actual situation because they are formed during several days, while active regions evolve.

Comparison of Figures 4a and 4b shows that the system of long loops revealed by the magnetic-field extrapolation (Figure 4b) corresponds to high coronal structures, indeed observed in EUV (Figure 4a). The GS source was associated with these long loops that connected the far-side flare site with the visible solar surface near the Equator. The γ -ray emission centroid position was close to the bases of these loops rooted on the visible side of the Sun.

The brown circle represents the refined > 100 MeV emission centroid position presented by Ajello et al. (2021a) in their Figure 5. Our result does not match this position probably because of the difference in the fish-eye-effect correction procedure and, possibly, a difference in some input parameters. Nevertheless, both Ajello et al. (2021a) and our result overlap in the region where the long loops connected to the far-side flare site were rooted to the visible solar surface.

These circumstances indicate that accelerated protons, just like electrons, could be injected from the flare site into the long loops and be trapped in them. A possible update of the scenario inferred by Grechnev et al. (2018) may be the escape little by little of trapped protons into the loss cone and their precipitation into dense layers of the solar atmosphere on the Earth-facing surface.

The stable γ -ray emission centroid position in the two temporal intervals separated by one hour corresponds more to the flare-related origin of accelerated protons than to their shock-related origin. In the latter case, the γ -ray emission centroid position would be expected to move across the solar disk (Plotnikov, Rouillard, and Share, 2017; Kouloumvakos et al., 2020).

4. Summary and Concluding Remarks

Following the methodology described by Ajello et al. (2014) and Ackermann et al. (2012, 2017), we have analyzed the high-energy γ -ray emission in the 1 September 2014 event and obtained the results that are close to those of the *Fermi*/LAT team. Our study confirms and clarifies their conclusions related to both methodological and physical aspects. In addition, we calculated the γ -ray emission centroid position during the second observational interval after the flare; it virtually coincides with the position in the first interval.

The outcome of our spectral analysis of the γ -ray emission in this event is consistent with the results of the *Fermi*/LAT team and different authors. This is particularly related to the

estimated proton power-law index of ≈ 4.7 during the flare and ≈ 3.7 during the late-phase emission.

The compensation for the fish-eye effect makes the calculated γ -ray emission centroid position practically insensitive to the low-energy threshold. The influence of the fish-eye effect was strong during the first flare interval and considerably weaker during the second, post-flare interval, when the LAT boresight was different. We also compared the results of localization using the `gttmap` and `gtfindsrc` procedures. The `gtfindsrc` seems a bit more accurate; the results differ slightly with a difference noticeably smaller than the 68% error radius.

The γ -ray emission centroid position during the flare that we found is close to the refined position in the LAT catalog (Ajello et al., 2021a). This position does not contradict the results of different studies. Notable is the persistence of the γ -ray source position in the two temporal intervals separated by one hour. Its proximity to the bases of the coronal loops connected to the flare site supports the flare-related origin of high-energy protons.

As mentioned, the > 100 MeV emission centroid positions for almost all of the events listed in the LAT catalog are remarkably close to their parent active regions. The 7 March 2012 event seems to be the only one whose γ -ray emission centroid position moved across the solar disk for several hours. This was another event for which we calculated the γ -ray emission centroid positions using the methodology described. Our results are close to the results of Ajello et al. (2021a) in all the temporal intervals they considered.

At first glance, the displacement of the γ -ray-emitting region seems to favor the shock-related origin of high-energy protons in the 7 March 2012 event. This event was addressed in detail by Ajello et al. (2014). After considering different scenarios, the authors concluded that high-energy γ -rays were most likely produced by energetic protons that were accelerated in the corona rather than by the CME-driven shock continuously during the whole duration of the emission. This conclusion is consistent with the following circumstance. As Hudson (2018) pointed out, a large mirror ratio at the base of an open coronal structure prevents the back-precipitation of particles from large coronal heights so that only a small part of the protons is able to return to the Sun. The simulations carried out by Hutchinson et al. (2022) also demonstrate that the CME-shock source scenario does not make it possible to obtain both long-duration γ -ray emission and efficient proton precipitation. Bruno et al. (2023) further elaborated on the challenges facing the CME-shock source scenario.

Future detailed analysis of the *Fermi*/LAT observations promises a deeper insight into long-standing challenges. Our results supplement the knowledge about the SOL2014-09-01 event. The present study also provides verification and clarification of the methodology for further analysis of this and other events from the *Fermi*/LAT data. We hope that our study would help the solar community to successfully use the *Fermi*/LAT observations that since 2008 have provided unique information on high-energy solar γ -ray emission.

Acknowledgments We thank the team members of the NASA's *Fermi Gamma-Ray Space Telescope* for their open policy and efforts to provide valuable information. We also thank the NASA/SDO and the AIA and HMI science teams, the Nançay Radioheliograph team, and the team of the SWAP telescope on the ESA's *Proba 2* micro-satellite. We are grateful to the anonymous reviewer for substantial remarks and helpful recommendations.

Author contributions A.A. Kochanov supervised the study, performed the calculations, and wrote the main part of the manuscript. V.I. Kiselev collected and analyzed the raw data, prepared tables, and participated in writing the manuscript. V.V. Grechnev and A.M. Uralov prepared figures, analyzed the results, wrote Section 3.2, and edited the text. All authors reviewed the manuscript.

Funding This study was financially supported by the Ministry of Science and Higher Education of the Russian Federation. The draft of Figure 4 with coronal structures was made with the support from the Russian Science Foundation under grant 18-12-00172.

Data Availability The datasets analyzed during the current study were derived from the following public domain resources:

The Fermi Gamma-ray Space Telescope fermi.gsfc.nasa.gov/.

Virtual Solar Observatory sdac.virtualsolar.org/.

The Proba2 Science Center proba2.sidc.be/swap/data/bsd/.

Radio Solar DataBase @ Nançay rsdb.obs-nancay.fr/.

Declarations

Competing interests The authors declare no competing interests.

References

- Abdo, A.A., Ackermann, M., Ajello, M., Atwood, W.B., Axelsson, M., Baldini, L., Ballet, J., Band, D.L., Barbiellini, G., Bastieri, D., et al.: 2009, Fermi/Large Area Telescope bright gamma-ray source list. *Astrophys. J. Suppl.* **183**, 46. [DOI](#). [ADS](#).
- Abdo, A.A., Ackermann, M., Ajello, M., Baldini, L., Ballet, J., Barbiellini, G., Bastieri, D., Bechtol, K., Bellazzini, R., Berenji, B., et al.: 2011, Fermi Large Area Telescope observations of two gamma-ray emission components from the quiescent Sun. *Astrophys. J.* **734**, 116. [DOI](#). [ADS](#).
- Ackermann, M., Ajello, M., Albert, A., Allafort, A., Atwood, W.B., Axelsson, M., Baldini, L., Ballet, J., Barbiellini, G., Bastieri, D., et al.: 2012, The Fermi Large Area Telescope on orbit: event classification, instrument response functions, and calibration. *Astrophys. J. Suppl.* **203**, 4. [DOI](#). [ADS](#).
- Ackermann, M., Allafort, A., Baldini, L., Barbiellini, G., Bastieri, D., Bellazzini, R., Bissaldi, E., Bonino, R., Bottacini, E., Bregeon, J., et al.: 2017, Fermi-LAT observations of high-energy behind-the-limb solar flares. *Astrophys. J.* **835**, 219. [DOI](#). [ADS](#).
- Ajello, M., Albert, A., Allafort, A., Baldini, L., Barbiellini, G., Bastieri, D., Bellazzini, R., Bissaldi, E., Bonamente, E., Brandt, T.J., et al.: 2014, Impulsive and long duration high-energy gamma-ray emission from the very bright 2012 March 7 solar flares. *Astrophys. J.* **789**, 20. [DOI](#). [ADS](#).
- Ajello, M., Baldini, L., Bastieri, D., Bellazzini, R., Berretta, A., Bissaldi, E., Blandford, R.D., Bonino, R., Bruel, P., Buson, S., et al.: 2021a, First Fermi-LAT solar flare catalog. *Astrophys. J. Suppl.* **252**, 13. [DOI](#). [ADS](#).
- Ajello, M., Baldini, L., Bastieri, D., Bellazzini, R., Berretta, A., Bissaldi, E., Blandford, R.D., Bonino, R., Bruel, P., Buson, S., et al.: 2021b, Erratum: first Fermi-LAT solar flare catalog (2021, ApJS, 252, 13). *Astrophys. J. Suppl.* **256**, 24. [DOI](#). [ADS](#).
- Akimov, V.V., Ambroz, P., Belov, A.V., Berlicki, A., Chertok, I.M., Karlický, M., Kurt, V.G., Leikov, N.G., Litvinenko, Y.E., Magun, A., Minko-Wasiluk, A., Rompolt, B., Somov, B.V.: 1996, Evidence for prolonged acceleration based on a detailed analysis of the long-duration solar gamma-ray flare of June 15, 1991. *Solar Phys.* **166**, 107. [DOI](#). [ADS](#).
- Atwood, W.B., Abdo, A.A., Ackermann, M., Althouse, W., Anderson, B., Axelsson, M., Baldini, L., Ballet, J., Band, D.L., Barbiellini, G., et al.: 2009, The Large Area Telescope on the Fermi gamma-ray space telescope mission. *Astrophys. J.* **697**, 1071. [DOI](#). [ADS](#).
- Berghmans, D., Hochedez, J.F., Defise, J.M., Lecat, J.H., Nicula, B., Slemzin, V., Lawrence, G., Katsiyannis, A.C., van der Linden, R., Zhukov, A., et al.: 2006, SWAP onboard PROBA 2, a new EUV imager for solar monitoring. *Adv. Space Res.* **38**, 1807. [DOI](#). [ADS](#).
- Bruno, A., de Nolfo, G.A., Ryan, J.M., Richardson, I.G., Dalla, S.: 2023, Statistical relationship between long-duration high-energy gamma-ray emission and solar energetic particles. *Astrophys. J.* **953**, 187. [DOI](#). [ADS](#).
- Chupp, E.L., Ryan, J.M.: 2009, High energy neutron and pion-decay gamma-ray emissions from solar flares. *Res. Astron. Astrophys.* **9**, 11. [DOI](#). [ADS](#).
- Chupp, E.L., Forrest, D.J., Ryan, J.M., Heslin, J., Reppin, C., Pinkau, K., Kanbach, G., Rieger, E., Share, G.H.: 1982, A direct observation of solar neutrons following the 0118 UT flare on 1980 June 21. *Astrophys. J. Lett.* **263**, L95. [DOI](#). [ADS](#).
- Cliver, E.W., Kahler, S.W., Vestrand, W.T.: 1993, On the origin of gamma-ray emission from the behind-the-limb flare on 29 September 1989. In: Leahy, D.A., Hicks, R.B., Venkatesan, D. (eds.) *Internat. Cosmic Ray Conf.* **3**, World Scientific, Singapore, 91. [ADS](#).
- Cohen, C.M.S., Mewaldt, R.A.: 2018, The ground-level enhancement event of September 2017 and other large solar energetic particle events of cycle 24. *Space Weather* **16**, 1616. [DOI](#). [ADS](#).

- Dermer, C.D.: 1986, Binary collision rates of relativistic thermal plasmas. II. Spectra. *Astrophys. J.* **307**, 47. DOI. ADS.
- Gopalswamy, N., Mäkelä, P., Yashiro, S., Akiyama, S., Xie, H., Thakur, N.: 2020, Source of energetic protons in the 2014 September 1 sustained gamma-ray emission event. *Solar Phys.* **295**, 18. DOI. ADS.
- Grechnev, V.V., Kiselev, V.I., Kashapova, L.K., Kochanov, A.A., Zimovets, I.V., Uralov, A.M., Nizamov, B.A., Grigorieva, I.Y., Golovin, D.V., Litvak, M.L., Mitrofanov, I.G., Sanin, A.B.: 2018, Radio, hard X-ray, and gamma-ray emissions associated with a far-side solar event. *Solar Phys.* **293**, 133. DOI. ADS.
- Hirasima, Y., Okudaira, K., Yamagami, T.: 1970, Solar gamma ray burst observed on 27 Sept. 1968. In: *Internat. Cosmic Ray Conf* **2**, 683. ADS.
- Hudson, H.S.: 2018, The relationship between long-duration gamma-ray flares and solar cosmic rays. In: Foullon, C., Malandraki, O.E. (eds.) *Space Weather of the Heliosphere: Processes and Forecasts* 335, 49. DOI. ADS.
- Hutchinson, A., Dalla, S., Laitinen, T., de Nolfo, G.A., Bruno, A., Ryan, J.M., Waterfall, C.O.G.: 2022, Energetic proton back-precipitation onto the solar atmosphere in relation to long-duration gamma-ray flares. *Astron. Astrophys.* **658**, A23. DOI. ADS.
- Jin, M., Petrosian, V., Liu, W., Nitta, N.V., Omodei, N., Rubio da Costa, F., Effenberger, F., Li, G., Pesce-Rollins, M., Allafort, A., Manchester IV, W.: 2018, Probing the puzzle of behind-the-limb γ -ray flares: data-driven simulations of magnetic connectivity and CME-driven shock evolution. *Astrophys. J.* **867**, 122. DOI. ADS.
- Kafexhiu, E., Romoli, C., Taylor, A.M., Aharonian, F.: 2018, Energetic gamma-ray emission from solar flares. *Astrophys. J.* **864**, 148. DOI. ADS.
- Kerdraon, A., Delouis, J.-M.: 1997, The Nançay Radioheliograph. In: Trottet, G. (ed.) *Coronal Physics from Radio and Space Observations* **483**, 192. DOI. ADS.
- Kouloumvakos, A., Rouillard, A.P., Share, G.H., Plotnikov, I., Murphy, R., Papaioannou, A., Wu, Y.: 2020, Evidence for a coronal shock wave origin for relativistic protons producing solar gamma-rays and observed by neutron monitors at Earth. *Astrophys. J.* **893**, 76. DOI. ADS.
- Lemen, J.R., Title, A.M., Akin, D.J., Boerner, P.F., Chou, C., Drake, J.F., Duncan, D.W., Edwards, C.G., Friedlaender, F.M., Heyman, G.F., et al.: 2012, The Atmospheric Imaging Assembly (AIA) on the Solar Dynamics Observatory (SDO). *Solar Phys.* **275**, 17. DOI. ADS.
- Lin, R.P., Dennis, B.R., Hurford, G.J., Smith, D.M., Zehnder, A., Harvey, P.R., Curtis, D.W., Pankow, D., Turin, P., Bester, M., et al.: 2002, The Reuven Ramaty High-Energy Solar Spectroscopic Imager (RHESSI). *Solar Phys.* **210**, 3. DOI. ADS.
- Longo, F., Iafate, G., Fermi LAT Collaboration: 2011, Solar flares monitor with Fermi-LAT. *Nucl. Instrum. Methods Phys. Res. A* **630**, 258. DOI. ADS.
- Mandzhavidze, N., Ramaty, R.: 1992, Gamma rays from pion decay – evidence for long-term trapping of particles in solar flares. *Astrophys. J. Lett.* **396**, L111. DOI. ADS.
- Mattox, J.R., Bertsch, D.L., Chiang, J., Dingus, B.L., Digel, S.W., Esposito, J.A., Fierro, J.M., Hartman, R.C., Hunter, S.D., Kanbach, G., et al.: 1996, The likelihood analysis of EGRET data. *Astrophys. J.* **461**, 396. DOI. ADS.
- Meegan, C., Lichti, G., Bhat, P.N., Bissaldi, E., Briggs, M.S., Connaughton, V., Diehl, R., Fishman, G., Greiner, J., Hoover, A.S., et al.: 2009, The Fermi Gamma-Ray Burst Monitor. *Astrophys. J.* **702**, 791. DOI. ADS.
- Murphy, R.J., Dermer, C.D., Ramaty, R.: 1987, High-energy processes in solar flares. *Astrophys. J. Suppl.* **63**, 721. DOI. ADS.
- Pesce-Rollins, M., Omodei, N., Petrosian, V., Liu, W., Rubio da Costa, F., Allafort, A., Chen, Q.: 2015a, First detection of > 100 MeV gamma-rays associated with a behind-the-limb solar flare. *Astrophys. J. Lett.* **805**, L15. DOI. ADS.
- Pesce-Rollins, M., Omodei, N., Petrosian, V., Liu, W., Rubio da Costa, F., Allafort, A., Fermi-LAT Collaboration: 2015b, Fermi Large Area Telescope observations of high-energy gamma-ray emission from behind-the-limb solar flares. In: *34th Internat. Cosmic Ray Conf. (ICRC2015)* **34**, 128. DOI. ADS.
- Pesnell, W.D., Thompson, B.J., Chamberlin, P.C.: 2012, The Solar Dynamics Observatory (SDO). *Solar Phys.* **275**, 3. DOI. ADS.
- Plotnikov, I., Rouillard, A.P., Share, G.H.: 2017, The magnetic connectivity of coronal shocks from behind-the-limb flares to the visible solar surface during γ -ray events. *Astron. Astrophys.* **608**, A43. DOI. ADS.
- Ryan, J.M.: 2000, Long-duration solar gamma-ray flares. *Space Sci. Rev.* **93**, 581. ADS.
- Scherrer, P.H., Schou, J., Bush, R.I., Kosovichev, A.G., Bogart, R.S., Hoeksema, J.T., Liu, Y., Duvall, T.L., Zhao, J., Title, A.M., et al.: 2012, The Helioseismic and Magnetic Imager (HMI) investigation for the Solar Dynamics Observatory (SDO). *Solar Phys.* **275**, 207. DOI. ADS.
- Schrijver, C.J., De Rosa, M.L.: 2003, Photospheric and heliospheric magnetic fields. *Solar Phys.* **212**, 165. DOI. ADS.

- Share, G.H., Murphy, R.J., White, S.M., Tolbert, A.K., Dennis, B.R., Schwartz, R.A., Smart, D.F., Shea, M.A.: 2018, Characteristics of late-phase >100 MeV gamma-ray emission in solar eruptive events. *Astrophys. J.* **869**, 182. DOI. ADS.
- Tolbert, K., Schwartz, R.: 2020, OSPEX: Object Spectral Executive. *Astrophys. Source Code Lib.* 2007.018. ADS.
- Vilmer, N., MacKinnon, A.L., Hurford, G.J.: 2011, Properties of energetic ions in the solar atmosphere from γ -ray and neutron observations. *Space Sci. Rev.* **159**, 167. DOI. ADS.
- Yashiro, S., Gopalswamy, N., Michalek, G., St. Cyr, O.C., Plunkett, S.P., Rich, N.B., Howard, R.A.: 2004, A catalog of white light coronal mass ejections observed by the SOHO spacecraft. *J. Geophys. Res. Space Phys.* **109**, A07105. DOI. ADS.

Publisher's Note Springer Nature remains neutral with regard to jurisdictional claims in published maps and institutional affiliations.

Springer Nature or its licensor (e.g. a society or other partner) holds exclusive rights to this article under a publishing agreement with the author(s) or other rightsholder(s); author self-archiving of the accepted manuscript version of this article is solely governed by the terms of such publishing agreement and applicable law.